Clays and Clay Minerals, Vol. 54, No. 4, 515–528, 2006.

PORE-SCALE ANALYSIS OF BULK VOLUME CHANGE FROM CRYSTALLINE INTERLAYER SWELLING IN Na^+- AND Ca^{2+}-SMECTITE

WILLIAM J. LIKOS[1,*] AND NING LU[2]

[1] University of Missouri-Columbia, Department of Civil and Environmental Engineering, Columbia, MO 65211, USA
[2] Colorado School of Mines, Engineering Division, Golden, CO 80401, USA

Abstract—Water-vapor sorption experiments were conducted to quantify bulk volume change of compacted expansive clay specimens resulting from interlayer hydration and dehydration in the crystalline swelling regime. Effects of interlayer cation type and pore fabric are examined by comparing results for natural Na^+-smectite and Ca^{2+}-smectite specimens compacted over a range of initial bulk densities. Transitions in interlayer hydration states are reflected in the general shape of the sorption isotherms and corresponding relationships between humidity and volume change. Hysteresis is observed in both the sorption and volume-change response. Volume change for Ca^{2+}-smectite specimens is significantly greater than for Na^+-smectite over the entire range of packing densities considered. Loosely compacted specimens result in less volume change for both clays. Results are interpreted in light of a conceptual framework based on previous SEM and TEM observations of particle and pore fabric for Na^+ and Ca^{2+} smectite at high suctions. A pore-scale microstructural model is developed to quantitatively assess changes in interlayer and interparticle void volume during hydration. Modeling suggests that the relatively small volume changes observed for Na^+-smectite are attributable to a reduction of interparticle void volume as expanding quasicrystals encroach into surrounding larger-scale pores. Volume change hysteresis is attributed to unrecovered alterations in interparticle fabric required to accommodate the swelling process. The results provide new insight to address volume change upscaling, hysteresis, and the general evolution of bi-modal pore fabric during crystalline swelling.

Key Words—Crystalline Swelling, Dehydration, Hydration, Interlayer, Smectite, Upscaling.

INTRODUCTION

Crystalline swelling is a process whereby expandable 2:1 phyllosilicates sequentially intercalate one, two, three or four discrete layers of H_2O molecules between the mineral interlayers (*e.g.* Norrish, 1954). The extent of crystalline swelling is controlled primarily by the energy associated with hydration of interlayer cations and charge sites counteracted by attractive forces from van der Waals and Coulombic electrostatic attraction between the negatively charged mineral layers and positively charged interlayer cations (*e.g.* Kittrick, 1969). Depending on the mineral surface charge and the predominant type of exchangeable cation, interlayer adsorption may proceed beyond the three or four molecular water layers associated with crystalline swelling under what is generally accepted to be an osmotic swelling mechanism. Transition from the crystalline swelling regime to the osmotic swelling regime occurs readily for monovalent clay-water-ion systems such as Na^+-smectite, which are characterized by relatively weak interlayer attractive forces, but does not readily occur for polyvalent systems such as Ca^{2+}-smectite, which are characterized by relatively strong interlayer forces (*e.g.* MacEwan and Wilson, 1980).

* E-mail address of corresponding author:
likosw@missouri.edu
DOI: 10.1346/CCMN.2006.0540412

Interlayer hydration and dehydration in the crystalline swelling regime has been explored by a number of researchers using a variety of approaches. Studies have taken the form, for example, of X-ray diffraction (XRD) analyses under controlled relative humidity (RH) conditions (*e.g.* Gillery, 1959; Del Pennino *et al.*, 1981; Huang *et al.*, 1994; Chipera *et al.*, 1997), mathematical considerations of interlayer geometry (*e.g.* Barshad, 1949), gravimetric and thermogravimetric sorption analyses (*e.g.* Mooney *et al.*, 2002; Collis-George, 1955; Keren and Shainberg, 1975; Cases *et al.*, 1992; Berend *et al.*, 1995), and investigations of interlayer water structure using infrared spectroscopy (*e.g.* Farmer and Russell 1971; Sposito and Prost 1982; Bishop *et al.* 1994), neutron diffraction (*e.g.* Cebula *et al.* 1979; Hawkins and Egelstaff 1980; Poinsignon *et al.* 1987; Powell *et al.* 1997), and NMR spectroscopy (*e.g.* Grandjean and Laszlo 1989; Delville and Letellier 1995; Weiss and Gerazimowicz 1996). Posner and Quirk (1964), Slade *et al.* (1991) and Slade and Quirk (1991) examined crystalline swelling processes in smectite under fully saturated conditions by controlling H_2O activity with variously concentrated salt solutions. Other research efforts have included macroscopic energy balance modeling (*e.g.* Laird, 1996) and, most recently, numerical simulations of mineral hydration using molecular dynamics and Monte Carlo methods (*e.g.* Boek *et al.*, 1995; Chang *et al.*, 1995; Karaborni *et al.*, 1997; Sposito *et al.*, 1999).

Numerous practical engineering and industrial applications provide motivation for examining the macroscopic (bulk) volume change behavior of expansive clay. Notable examples include mitigating damage to civil infrastructure founded on expansive soils, understanding borehole stability issues in shale, and preventing the development of tension cracks in waste containment or buffer systems consisting of expansive clay. Efforts to address these types of issues have historically focused on measuring or predicting volume change and associated swelling pressure within the osmotic swelling regime (*e.g.* by measuring the behavior of specimens completely inundated with pore fluid in one-dimensional oedometer systems). Very few studies, however, have explored bulk swelling behavior within the crystalline swelling regime. The studies summarized in the previous paragraph afford a significantly greater understanding of crystalline swelling at the relatively microscopic scale of the mineral interlayer. However, there is a disparate amount of experimental or theoretical evidence available to investigate how interlayer volume changes upscale to macroscopic volume changes for clay systems composed of multiple interacting particles. Previous studies have clarified many of the important mineralogical and physicochemical controls on crystalline swelling, including the influences of layer charge, charge site location, and interlayer cation type. However, the macroscopic variables necessarily introduced by upscaling from the particle scale to the multiparticle scale remain relatively uncertain (*e.g.* particle size, particle fabric, confining pressure).

METHODS AND MATERIALS

The experimental focus of this work is on measuring bulk volume changes from interlayer crystalline swelling processes in smectite. Relative humidity is controlled in an environmental chamber for a series of 'multi-step' sorption experiments and using salt solutions for a series of 'single-step' sorption experiments. Compacted clay specimens are placed in the controlled-humidity environments for measuring equilibrium water content and bulk volume changes over RH ranging from near zero to ~85% along wetting and drying paths. The effects of interlayer cation type and pore fabric are examined by comparing the results for natural Na^+- and Ca^{2+}-smectite specimens compacted over a range of initial void ratios. The results are analyzed in light of a qualitative conceptual model for the pore and particle fabric of Na^+- and Ca^{2+}-smectite and a quantitative microstructural model developed to estimate interlayer and interparticle pore volume and their evolution during interlayer hydration.

The first author has previously described a laboratory experimental system for measuring relationships among RH, gravimetric water content, and the corresponding macroscopic volume change of compacted clay specimens within the crystalline swelling regime (Likos, 2004). The system is capable of actively controlling RH between ~0.5% and 90% along either wetting or drying paths in a small environmental chamber by combining vapor-saturated and desiccated N_2 gas streams. Compacted cylindrical clay specimens are placed in the chamber and monitored for changes in mass and height under imposed changes in RH. Steady-state values are used to calculate gravimetric water content (w) and axial strain (ε_a) by referencing the measured mass and height to initial values at a baseline oven-dried condition. Increments in water content and axial strain are plotted as functions of RH to generate characteristic sorption and volume change isotherms along wetting and subsequent drying paths.

An initial series of specimens was formed from the minus #200 (75 μm) fraction of Wyoming bentonite. X-ray diffraction patterns were obtained for evaporated sample mounts using an automated Scintag XDS-2000 XRD system employing CuKα radiation. All samples were scanned from 2 to 35º2θ with a stepsize of 0.02º2θ. Heat and ethylene glycol treatments were performed according to procedures described by Moore and Reynolds (1997). Analysis of the XRD patterns (Figure 1a) indicates that the Wyoming clay consists predominantly of discrete smectite with a minor quartz component. The sharp reflection evident in the air-dry pattern at ~9.7º2θ and to a lesser extent at 15.8º2θ indicates the presence of zeolite. The cation exchange capacity (CEC) determined using ammonium displacement was 66 meq/100 g, consisting predominantly of Na^+. Liquid and plastic limits were determined following the procedures described in ASTM D4318 (ASTM, 2000) to be 485% and 132%, respectively. These relatively high values, in addition to the location of the $S(001)_{air}$ peak at 7.1º2θ (12.4 Å), reflect the predominance of Na^+ in the exchange complex.

A second series of specimens was formed from the minus #200 fraction of natural clay sampled from a thin bentonite seam within an outcrop of the Graneros Shale located southwest of Golden, Colorado. This material consisted primarily of discrete smectite with trace amounts of kaolinite and non-clay minerals (Figure 1b). The total CEC was 82 meq/100 g, consisting predominantly of Ca^{2+} and Mg^{2+}. Liquid and plastic limits for the Colorado clay were 118% and 45%, respectively. These relatively low values, in addition to the location of the $S(001)_{air}$ peak at 6.0º2θ (14.7 Å), reflect the predominance of divalent cations in the exchange complex. For simplicity, the Wyoming and Colorado clays are referred to herein as Na^+- smectite and Ca^{2+}-smectite, respectively.

The mean thicknesses of the smectite crystallites were estimated using the Fourier decomposition technique of Bertaut-Warren-Averbach applied to the XRD patterns for the glycolated clays (MudMaster program; Eberl *et al.* (1996)). The XRD patterns were analyzed for

https://doi.org/10.1346/CCMN.2006.0540412 Published online by Cambridge University Press

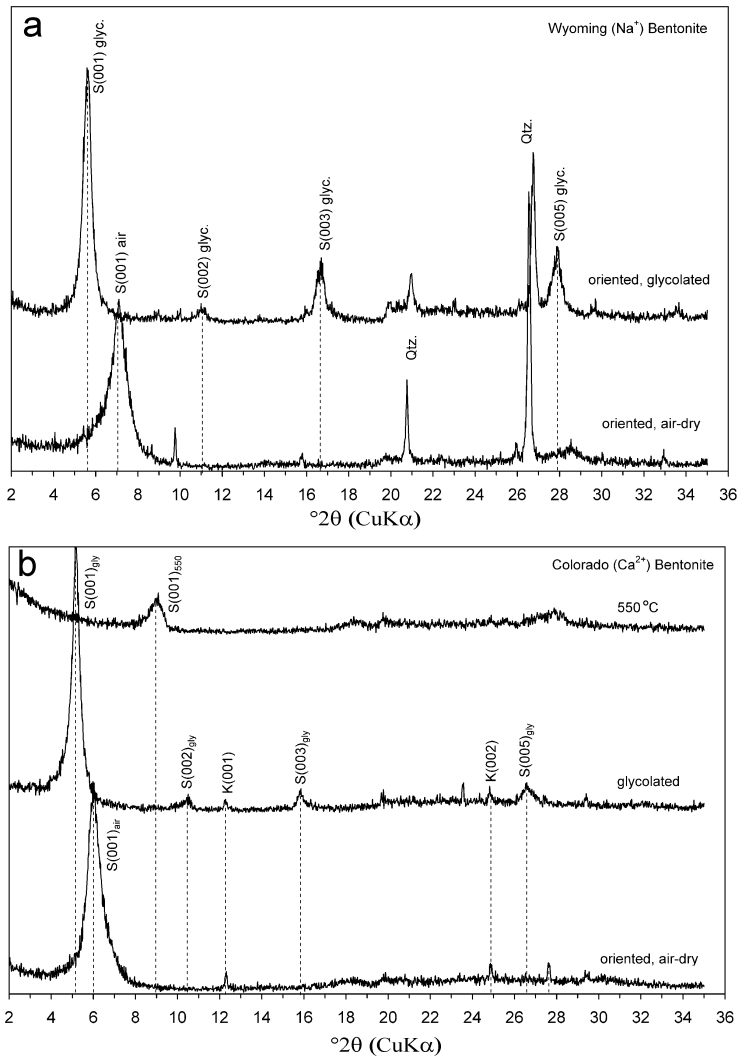

Figure 1. XRD patterns (CuKα): (a) Na^{+}-smectite, and (b) Ca^{2+}-smectite.

the smectite 001 reflections from 3.5 to 7.5 Å with no smoothing applied. Extrapolated mean crystallite thicknesses ($\bar{T}_c$) were 12.7 nm and 11.1 nm for the Na^{+} and Ca^{2+} specimens, respectively, which correspond to a mean of 7.6 and 6.6 expandable layers (m) per crystallite. These values are near the upper limit reported by Mystkowski *et al.* (2000) for a wide range of natural smectites ($3.4 \leqslant m \leqslant 7.3$).

Compacted specimens were prepared by compressing ~10 g of oven-dried (105ºC) clay into a lubricated 3.78 cm diameter mold using a 50 kN capacity load frame. As indicated in Figure 2, the magnitude of applied compaction pressure was varied to produce specimens with a wide range of initial void ratios. Specimens were extruded from the compaction mold using a piston assembly, oven dried a second time to constant mass at 105ºC, and initial height h_i was measured to ±0.0001 cm using a micrometer assembly.

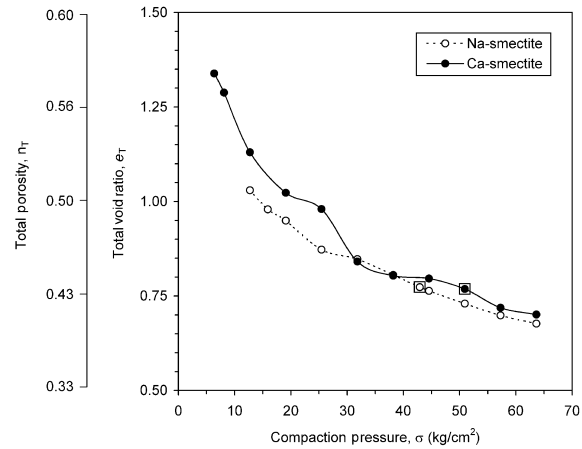

Figure 2. Relationship between total void ratio and compaction pressure for Na^{+}- and Ca^{2+}-test specimens. The two highlighted specimens were used for multi-step sorption testing. All others were used for single-step sorption testing.

https://doi.org/10.1346/CCMN.2006.0540412 Published online by Cambridge University Press

The two specimens highlighted in Figure 2 at a void ratio of ~e = 0.77 were selected for 'multi-step' sorption and volume change testing in the humidity-controlled environmental chamber so that the response of Na^+ and Ca^{2+} specimens prepared to a similar bulk density could be directly compared. Relative humidity was ramped in increments of ~10% RH from near zero to a maximum near 85% RH and down again in similar increments along a desorption path. For comparison, two additional sorption isotherms were obtained using uncompacted Na^+ and Ca^{2+} specimens prepared by sprinkling 0.3–0.5 g of oven-dried clay onto a glass slide and then lightly compressing it with a second glass slide to an overall height of ~2 mm. Calibrations using an empty glass slide showed that the amount of water adsorbed by the blank at 90% RH was negligible (<0.0001 g). Specimen axial deformation and mass for the compacted specimens were recorded after steady state was reached for each RH increment. Axial strain was calculated as the change in specimen height Δh measured at its center using a linear displacement transducer (LVDT) divided by its baseline height h_i prior to sorption ($\varepsilon_a = \Delta h/h_i \times 100\%$). Output from the LVDT was acquired at a resolution of 7.38 μm, which translates to a resolution in ε_a of ~0.15% for a typical initial specimen height equal to ~0.5 cm. The amount of time required for steady state generally increased with increasing RH and ranged from ~75 to 150 h per step. Approximately 70 days were required for completion of the entire 20- to 25-step wetting-drying cycle. Isotherms were obtained at a mean temperature of 24ºC with a standard deviation of 0.1ºC over the duration. Specimens were unconfined laterally and no axial surcharge was applied (*i.e.* free swelling conditions). Radial specimen deformations (Δr) were not measured but may be inferred by assuming that volume change under free swelling conditions occurs isotropically and that the radial (ε_r) and axial strain (ε_a) are equal (*e.g.* Delage *et al.*, 1998).

The remaining compacted specimens were retained for a series of 'single-step' sorption tests using salt (NaCl) solutions to control RH at a constant and relatively high value (RH ≈ 93%). The specimens were initially oven dried to establish baseline conditions and then placed in the headspace of a fritted glass dessicator over a 2.0 M NaCl solution, which produced RH of ~93% measured using a thin-film capacitance sensor. Relatively high humidity conditions were chosen to generate an environment corresponding to near the upper limit of the two-layer hydration state for both clays. Specimens were removed after 10–15 days and equilibrium height and mass were measured using a micrometer assembly and electronic balance, respectively. Measurements were referenced to initial values at baseline conditions to compute axial strain and gravimetric water content at RH ~93%. All specimens for the single-step sorption series were unconfined both axially and radially.

RESULTS AND DISCUSSION

Sorption isotherms

Figure 3 shows water-vapor sorption isotherms obtained from the multi-step testing series for uncompacted and compacted (e_i = 0.77) Na^+ and Ca^{2+} specimens. The isotherm for the compacted Na^+ specimen was obtained along a wetting-drying path from ~3% RH, to a maximum of 85% RH and back to a minimum of 11% RH. The isotherm for the compacted Ca^{2+} specimen was obtained along a similar wetting-drying path, but testing was interrupted during drying at 37% RH due to a power failure in the laboratory. Gravimetric water content at maximum RH are 15.5% and 18.0% for the compacted Na^+ and Ca^{2+} specimens, respectively. Isotherms for uncompacted specimens were obtained to a maximum of 92.3% RH and 89.4% RH. Hysteresis is

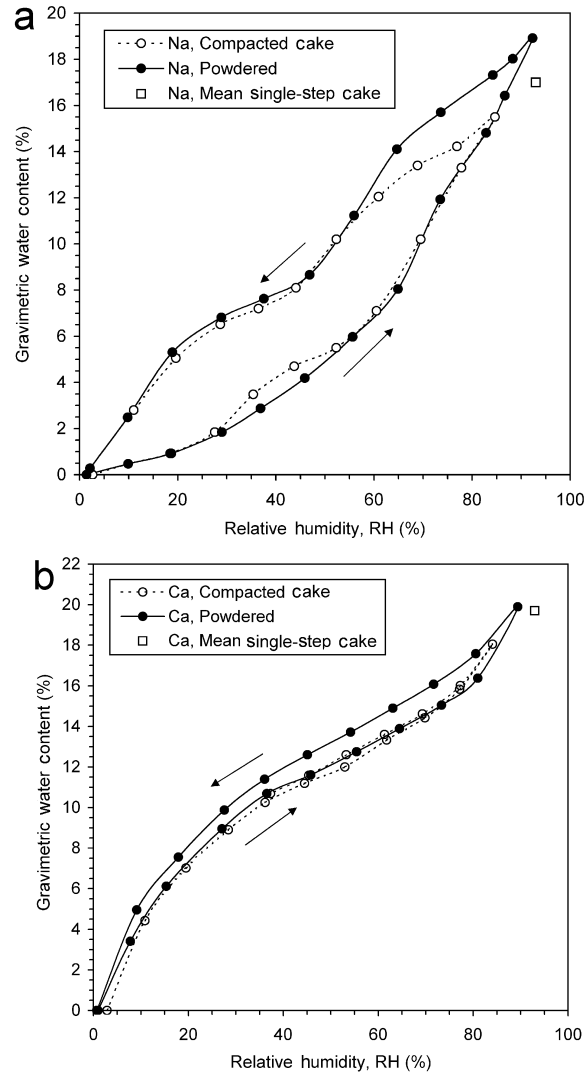

Figure 3. Water-vapor sorption isotherms from multi-step testing series: (a) Na^+-smectite and (b) Ca^{2+}-smectite. Arrows denote direction of wetting.

https://doi.org/10.1346/CCMN.2006.0540412 Published online by Cambridge University Press

evident in the isotherms for the Na^+ specimens and to a lesser extent for the Ca^{2+} specimens. The nature of the hysteresis, where more water is retained during drying than during previous wetting, is consistent with the sorption behavior of expansive clay and more general porous media in the literature.

The amount of water adsorbed by the Ca^{2+} specimen is greater than for the Na^+ specimen over the entire measured range of RH, supporting previous observations for RH values <~85–90% and reflecting the relatively high forces of initial hydration associated with the Ca^{2+} system (*e.g.* Mooney *et al.*, 2002; Keren and Shainberg, 1975). The BET analysis of the isotherms for the powdered specimens during initial wetting (RH <40%) indicates that monolayer coverage for the Na^+- and Ca^{2+}-smectite are 24 mg H_2O/g clay and 85 mg H_2O/g clay, respectively. Associated heats of adsorption are 0.40 kcal/mole and 1.46 kcal/mole, in good agreement with values reported by Keren and Shainberg (1975) for Na^+- and Ca^{2+}-exchanged Wyoming bentonite. Heats of adsorption calculated from the desorption isotherms (RH <40%) are 1.91 kcal/mole and 1.40 kcal/mole for the Na^+ and Ca^{2+} specimens, respectively.

Previous XRD studies have indicated that Na^+-smectite transitions through the zero- (d_{001} ~9.7 Å), one- (~12 Å), and two-layer (~15.5 Å) hydration states when RH is increased from 0 to ~90%. Transitions from zero-to-one and from one-to-two layers occur within RH regimes ranging from ~10–40% and 50–90% RH, respectively. Interlayer spacing is relatively stable within RH domains between the transitions. Ca^{2+}-smectite has been shown to retain one water layer at RH even approaching 0%, transition to the two-layer state by RH of ~25%, and remains stable at the two-layer state as RH approaches ~90%. Transitions in basal spacing have also been shown to exhibit hysteresis between adsorption and desorption cycles, where larger interlayer separations are maintained to lower RH or H_2O activity values during desorption (*e.g.* Chipera *et al.*, 1997; Laird *et al.*, 1995).

The sorption isotherms for Na^+-smectite and to a lesser extent the Ca^{2+}-smectite (Figure 3) are characterized by relatively 'steep' portions, where a large amount of water is either gained or lost with a given change in humidity, as well as relatively 'flat' portions, where a lesser amount of water is gained or lost. This characteristic type of isotherm behavior is described more generally by Rouquerol (1999) as "wavy with an ill-defined double step" and has been documented extensively in the literature for expandable clay minerals including smectite and vermiculite (*e.g.* Mooney *et al.*, 1952; Collis-George, 1955; Cases *et al.*, 1992; Berend *et al.*, 1995). The characteristic has been interpreted as a manifestation of crystalline interlayer swelling, where the relatively steep portions indicate transitions from one particular hydration state to an adjacent hydration state. The relatively flat portions correspond to stable RH domains. The ill-defined nature of the transitions and stability domains may reflect concurrent adsorption on external surfaces in the larger-scale pore space and/or interstratification of hydration states among various interlayers and interlayer groups (*e.g.* Berend *et al.*, 1995).

Considering this interpretation of isotherm shape and the evidence from previous XRD studies, the relatively steep portion noted on the wetting loop of the Na^+-smectite isotherm (Figure 3a) between ~30% and 50% RH is interpreted to correspond to transition from the zero-layer hydrate state to the one-layer hydrate state. The relatively steep portion between ~60% and 85% RH corresponds to transition from the one-layer state to the two-layer state. These transitions are offset to lower ranges of RH during drying, which is consistent with the XRD observations. The relatively steep portion of the isotherm for the Ca^{2+}-smectite (Figure 3b) for RH <~30% is interpreted to reflect the one-to-two layer transition. The XRD evidence indicates that the two-layer state is relatively stable for RH up to ~85%. The significant adsorption that is evident in the isotherm beyond 30% RH, therefore, is interpreted to reflect additional water being adsorbed in the larger-scale interparticle pore space, which is supported subsequently by considering the bulk volume changes that occur.

Bulk volume change

Figure 4 is a plot of equilibrium axial strain as a function of RH during the wetting-drying cycles for compacted Na^+ and Ca^{2+} specimens tested in the multi-step environmental chamber. A maximum axial strain of 16.3% was recorded at the highest increment in RH for the Na^+ specimen. Maximum axial strain of 26.4% was recorded for the Ca^{2+} specimen. Corresponding volu-

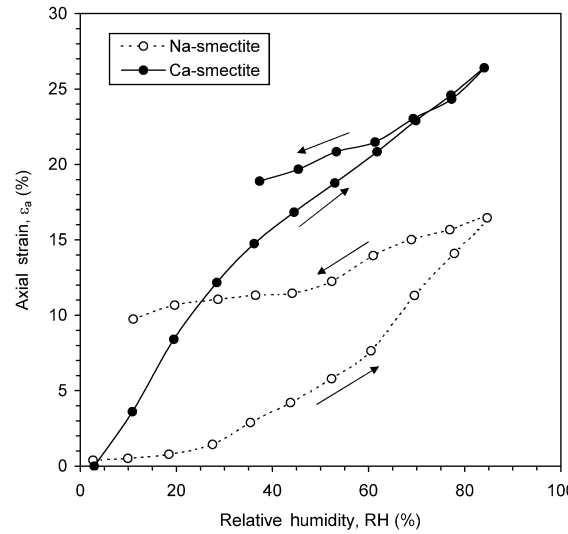

Figure 4. Steady-state axial strain measured during a multi-step wetting-drying cycle.

https://doi.org/10.1346/CCMN.2006.0540412 Published online by Cambridge University Press

metric strains (ε_v) for isotropic swelling are 57.9% and 102.0%, respectively. Hysteresis is evident over the full range of the wetting-drying cycle for the Na^+-smectite and over a portion (RH <60%) of the incomplete wetting-drying cycle for the Ca^{2+}-smectite. In both cases, axial strain is greater during drying than for the same value of RH during wetting, indicating that unrecovered volume changes were sustained along the drying paths. The amount of unrecovered volume is significantly greater for the Na^+-smectite than for the Ca^{2+}-smectite at comparable values of RH.

The axial strain response reflects the wavy behavior noted in the sorption isotherms. To illustrate, Figure 5 shows a derivative form of the volume change response as the slope of the relationship between axial deformation and relative humidity ($\Delta h/\Delta RH$). During wetting, the Na^+-smectite response (Figure 5a) exhibits two distinct peaks at RH of ~35% and 70% RH. These peaks are bounded by RH ranging from ~25% to 45% for the first, and from about 60% to 80% for the second. During drying, one peak is located at ~50% and bounded by RH from 40% to 70%. An additional peak is apparent near 10% RH but may not be fully defined due to the limited data range. The Ca^{2+}-smectite response (Figure 5b) exhibits a clear peak during wetting at ~20% RH bounded by RH of <45%. The magnitude of this peak ($\Delta h/\Delta RH = 0.032$) is significantly greater than the peaks observed in the Na^+-smectite response. The small peaks during drying are attributed to scatter resulting from the relatively small changes in specimen height occurring along the drying path.

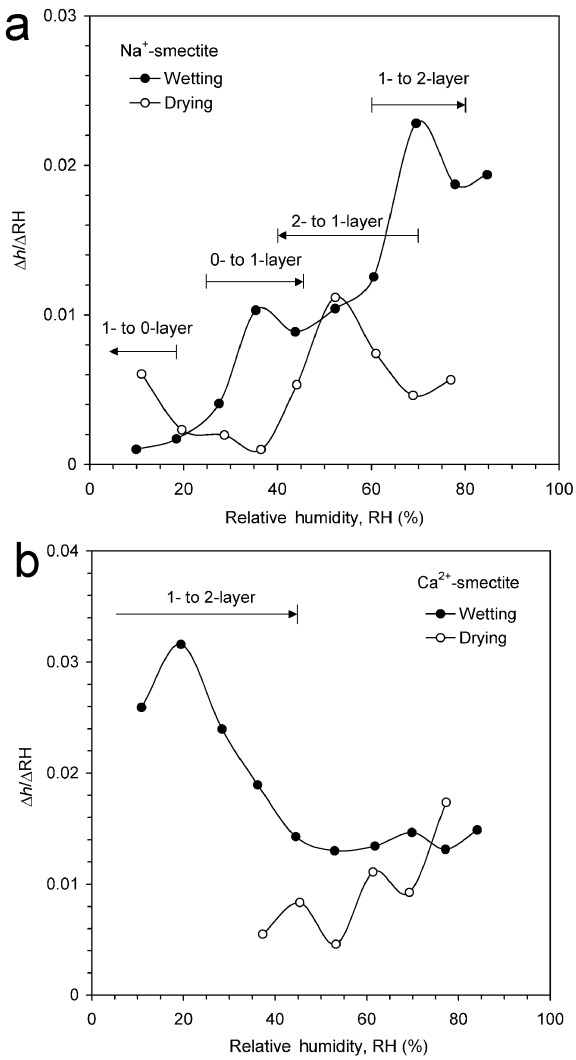

Figure 5. Slope of measured axial deformation – RH relationships as function of RH: (a) Na^+-smectite and (b) Ca^{2+}-smectite.

Peaks in $\Delta h/\Delta RH$ identify humidity regimes where a relatively large amount of macroscopic swell or shrinkage occurs. The locations of the major peaks correspond reasonably well with the relatively steep portions of the sorption isotherms noted on Figure 3 and with the basal spacing transition regimes evident in previous XRD results. We interpret the volume change associated with these peaks as the macroscopic manifestation of crystalline swelling. Specifically, the first peak for the Na^+-smectite during wetting (~35% RH) is interpreted to indicate volume change associated with transition of interlayer spacing from the zero-layer to the one-layer hydrate state. The peak at 70% RH indicates transition from the one-layer to the two-layer state. Both peaks are offset to lower RH values during drying, supporting the interpretation that these peaks are associated with the two-to-one and one-to-zero layer transitions. The large peak in $\Delta h/\Delta RH$ for the Ca^{2+}-smectite at ~20% RH is interpreted to reflect transition from the one-layer hydrate state to the two-layer hydrate state. The relatively large magnitude of this peak suggests that the interlayer volume change associated with the one-to-two layer transition is most effectively upscaled to macroscopic volume change.

Conceptual model for role of microstructure on bulk volume change

Figure 6 shows results obtained from the single-step sorption testing series in the form of equilibrium axial strain (%) measured at 93% RH as a function of the initial total void ratio of statically compacted Ca^{2+} and Na^+ specimens. Equilibrium water content of the ten Na^+ specimens ranged from 0.167 g/g to 0.173 g/g, with a mean of 0.170 g/g and standard deviation of 0.002 g/g. Equilibrium water content of the eight Ca^{2+} specimens ranged from 0.190 g/g to 0.199 g/g, with a mean of 0.197 g/g and standard deviation of 0.003 g/g. Mean values from the single-step series are included in Figure 3 for direct comparison with preceding results from the multistep sorption testing series and are in good agreement.

General observations are as follows: (1) larger initial void ratios (*i.e.* loose particle packing) result in lesser amounts of bulk volume change for both clay types;

https://doi.org/10.1346/CCMN.2006.0540412 Published online by Cambridge University Press

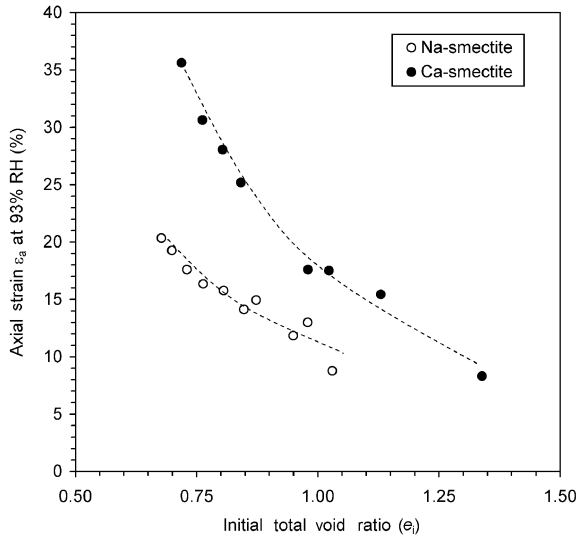

Figure 6. Axial strain at 93% RH as a function of initial total void ratio from a single-step testing series.

(2) volume change for the Ca^{2+}-smectite is significantly greater than for the Na^{+}-smectite over the overlapping range of initial void ratios considered; and (3) the difference in volume change between the Ca^{2+} and Na^{+} specimens tends to be greater at lower void ratios (*i.e.* dense particle packing). These observations illustrate the important influence of particle and pore fabric (microstructure) on the magnitude of bulk volume change attributable to crystalline swelling. Both clays are near the upper limit of the 2-layer hydrate state at 93% RH, which suggests that the differences observed in their bulk volume change response are not attributable to differences in the extent of interlayer hydration, but rather are attributable to differences in their basic fabric features.

Tessier (1990) describes the use of scanning (SEM) and transmission (TEM) electron microscopy and low-angle X-ray scattering to observe changes in the microstructure of homoionic smectites subject to a range of applied suction pressures and wetting-drying paths. Microstructure was characterized by three types of porosity corresponding to increasing magnitudes of scale: that between individual mineral layers (~9 Å), that corresponding to discontinuities between face-to-face oriented sub-stacks of mineral layers (~30–40 Å), and that between larger-scale "quasicrystals" (Aylmore and Quirk, 1971) consisting of multiple oriented sub-stacks (~1 μm). At low suction pressures (0.032 bar) and correspondingly high water contents, the microstructures of Ca^{2+}, Na^{+} (and Mg^{2+}) -smectite were noted to be similar, consisting of a network of 'walls' formed by quasicrystals enclosing the largest pore units. The number of mineral layers making up the walls, however, is generally larger for Ca^{2+}-smectite than for Na^{+} -smectite and increases with increasing suction pressure, reaching as many as 400 face-to-face oriented layers for Ca^{2+}-smectite and ~20 layers for Na^{+}-smectite at 1000 bar (~48% RH).

As illustrated in Figure 7, the fabric of the Ca^{2+}-smectite particle system (Figure 7a) prior to hydration may be considered to be defined by relatively thick network walls formed from quasicrystals comprising several face-to-face oriented sub-stacks of individual mineral layers. The sub-stacks each contain ~7–8 mineral layers, which was proved by the preceding MudMaster analysis (m = 7.6 and 6.6 layers for the Na^{+} and Ca^{2+} specimens, respectively) and is supported by TEM observations (Tessier, 1990). The total number of mineral layers comprising the quasicrystals for the Ca^{2+} system is perhaps of the order of 400. The Na^{+}-smectite fabric (Figure 7b), on the other hand, may be considered to have much thinner network walls, each comprising a lesser number of sub-stacks and a correspondingly smaller total number of mineral layers. The total number of mineral layers comprising the quasicrystals for the Na^{+} system is perhaps on the order of 20. The lateral extent of the quasicrystals is greater in the Ca^{2+} system than in the Na^{+} system as a result of the preferred face-to-face bonding in the former.

The total porosity of either fabric system reflects contributions from the interlayer pore space and the interparticle pore space. Here, we define the former as that associated with pore volume internal to the quasicrystals, thus including interlayer basal spacing and the intermediate pore space between the 7- to 8-layer sub-stacks. The latter is associated with pore space contributed by the larger scale voids enclosed by the quasicrystal network walls. Increases in basal spacing from crystalline swelling occur on the relatively microscopic scale defined within the quasicrystals (*i.e.* the interlayer pore space). As crystalline swelling proceeds, the volume of an individual quasicrystal increases to an extent that is dependent on the hydration state of the interlayers and the number of mineral layers comprising that quasicrystal.

This general fabric model and the discrepancies noted by Tessier (1990) in the high-suction microstructural features of Ca^{2+}- and Na^{+}-smectite provide a useful conceptual framework to explain the macroscale volume change behavior observed in the present work. We postulate that the efficiency with which interlayer volume changes translate or upscale to macroscopic volume changes depends on the relative volume of interlayer and interparticle voids, the size and structure of the basic particle units (quasicrystals), and the size, distribution, and connectivity of the interparticle voids. Particle fabrics or compaction conditions where the interparticle voids comprise a significant portion of the total void space or where the interparticle voids are well distributed and interconnected result in less bulk volume change because the increases in quasicrystal volume are more effectively adsorbed by the surrounding larger-scale pores. Conversely, particle fabrics where the

https://doi.org/10.1346/CCMN.2006.0540412 Published online by Cambridge University Press

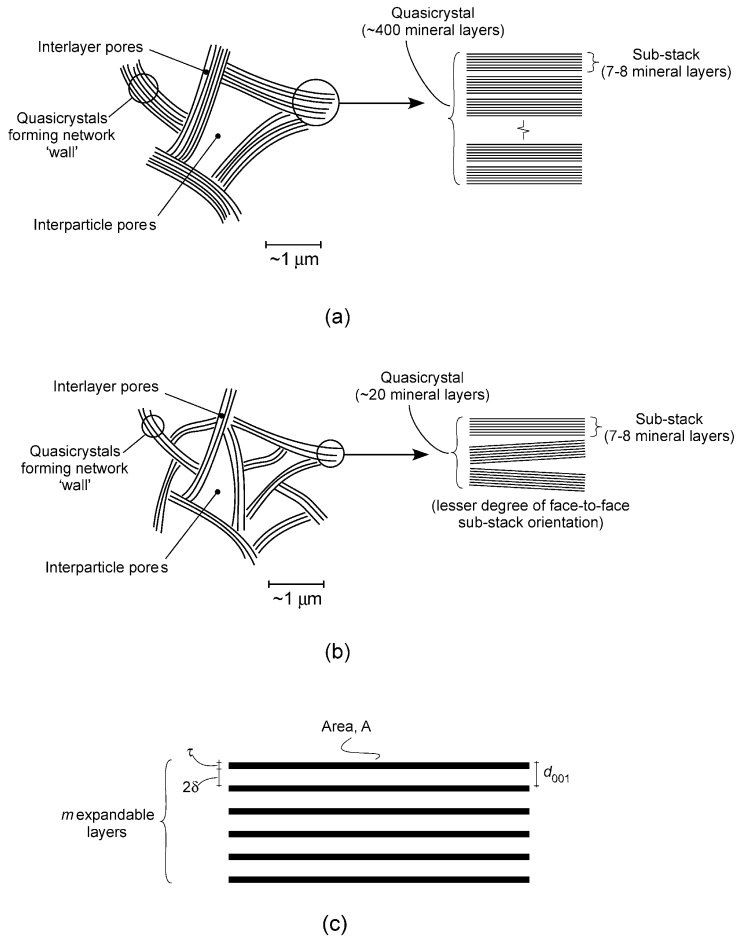

Figure 7. Conceptual microstructures for (a) Ca^{2+}-smectite and (b) Na^{+}-smectite. (c) Features of an individual quasicrystal for the quantitative microstructural model.

interparticle voids represent a smaller fraction of the total voids or where the interparticle voids are less well distributed and interconnected result in more efficient upscaling of the microscale scale changes in quasicrystal volume and more bulk volume change.

Compacting specimens by applying external stress results primarily in a reduction of interparticle pore space, thereby decreasing the ratio of interparticle-to-interlayer void volume. This loss of interparticle volume increases the efficiency of volume-change upscaling, which is evident from the first observation noted from results of our single-step tests on compacted specimens (larger initial void ratios result in lesser amounts of bulk volume change for both clay types). The observation that volume change for the Ca^{2+} system is greater than for the Na^{+}-smectite may be explained as follows. For Ca^{2+} and Na^{+} specimens compacted to the same total void ratio, the interparticle voids in the Na^{+} system represent a greater fraction of the total void volume, are well distributed among the relatively thin quasicrystals, and are therefore likely to be well connected in three dimensions. Thus, interlayer volume changes are more effectively absorbed by the interparticle void space and the translation of crystalline swelling to macroscopic volume change is inefficient. For the compacted Ca^{2+} system, where the interparticle voids represent a smaller fraction of the total void volume, are less well distributed, and may be more isolated, interlayer volume changes are less effectively absorbed by the interparticle void space and upscaling to macroscopic volume change is more efficient. The difference in bulk-volume change between the Ca^{2+} and Na^{+} specimens tends to be greater at lower total void ratios (the third observation) because the ratio of interparticle to interlayer void space is at a minimum. Larger initial void ratios result in lesser amounts of bulk volume change for both clay types because the ratio of interparticle to interlayer void space is at a maximum. These qualitative interpretations are supported by considering the evolution of interlayer and interparticle pore fabric in a quantitative sense.

Quantitative model for the role of microstructure in bulk volume change

In this section, we extend the conceptual fabric model to quantitatively assess changes in interlayer void volume resulting from crystalline swelling, associated

https://doi.org/10.1346/CCMN.2006.0540412 Published online by Cambridge University Press

changes in interparticle void volume, and how these changes affect upscaling to macroscopic volume changes for different compaction conditions. The pore structure of compacted expansive clay is considered to reside on two levels of scale: an interlayer scale defined by pore volume between individual mineral layers, and an interparticle scale defined by pore volume between and among individual quasicrystals. Thus, total void ratio (e_T) may be divided into additive terms representing an interparticle (e_{IP}) and interlayer (e_{IL}) component:

$$e_T = e_{IP} + e_{IL} \tag{1a}$$

where the total and component void ratios are defined as the ratio of void volume (V_v), interlayer volume (V_{IL}), and interparticle volume (V_{IP}) to the total volume of the mineral solids (V_s).

$$\frac{V_v}{V_s} = \frac{V_{IP}}{V_s} + \frac{V_{IL}}{V_s} = \frac{V_{IP} + V_{IL}}{V_s} \tag{1b}$$

Total interlayer volume V_{IL} is the product of the interlayer volume for an individual quasicrystal V_{ILi} and the number of quasicrystals N comprising the specimen:

$$V_{IL} = \sum_i V_{ILi} = V_{ILi} N \tag{2}$$

The interlayer volume of an individual quasicrystal with area A (m^2), interlayer separation distance 2δ (m), and m expandable layers (Figure 7c) is

$$V_{IL} = A\ 2\delta m \tag{3}$$

and the volume of solids comprising an individual quasicrystal is

$$V_{si} = A\ \tau\ m \tag{4}$$

where τ is the mineral sheet thickness (m). The number of quasicrystals N may be estimated from the ratio of the total mass of the specimen solids (m_{st}) and the mass of an individual quasicrystal (m_{si}):

$$N = \frac{m_{st}}{m_{si}} \tag{5}$$

where m_{st} is equal to the total mass of the specimen if it is initially dry. The mass of an individual quasicrystal comprising a dry specimen ($2\delta = 0$) can be calculated from the specific gravity of the mineral solids G_s and the quasicrystal volume V_{si} as follows:

$$m_{si} = G_s \rho_w A \tau m \tag{6}$$

where ρ_w is the density of water (g m^{-3}). Combining equations 5 and 6, an expression for the number of particles is:

$$N = \frac{m_{st}}{G_s \rho_w A \tau m} \tag{7}$$

which leads to the following expression for interlayer void ratio:

$$e_{IL} = \frac{V_{IL}}{V_s} = \frac{V_{ILi} N}{V_{si} N} = \frac{2\delta}{\tau} \tag{8}$$

Considering equation 1a, we have

$$e_T = e_{IP} + \frac{2\delta}{\tau} \tag{9}$$

which may also be written in incremental form to assess the changes in total void ratio that result from changes in interparticle and interlayer volume during crystalline swelling:

$$\Delta e_T = \Delta e_{IP} + \frac{\Delta 2\delta}{\tau} \tag{10}$$

The total void ratio may be determined at any point during the swelling process by measuring specimen volume and corresponding gravimetric water content. Interlayer void ratio may be determined from mean separation distance as a function of RH, which may be estimated by assigning RH ranges for the transition and stability of various hydration states or may be measured directly using XRD. Interparticle void ratio is equal to the total void ratio if the specimen is initially dry (*i.e.* $e_{IL} = 0$) and is equal to the difference in the measured total and interlayer void ratios during subsequent hydration.

Relative changes in interlayer and interparticle volume have an important influence on the translation of crystalline swelling to bulk volume change and the corresponding development of swelling pressure if the system is confined. Changes in interlayer volume are generally positive for a swelling process, which reflect the increasing interlayer separation. Changes in interparticle volume, on the other hand, may be either positive or negative, where the latter case reflects a loss of interparticle voids that may occur as the swelling quasicrystals encroach into their surrounding void space. For fully confined specimens, the total volume remains constant and the increase in interlayer volume is offset by an equivalent decrease in interparticle volume. This results in an exertion of a maximum swelling pressure on the confining system. For partially confined specimens (*i.e.* applied stress < maximum swelling pressure), the increase in interlayer volume may or may not be offset by an equivalent decrease in interparticle volume. If the stress required to reduce the interparticle void volume is greater than the applied confining pressure, macroscopic volume change occurs. Under free swelling conditions, losses in interparticle volume are minimized and the corresponding potential for macroscopic volume change is at a maximum. In each of these cases, the extent to which changes in interlayer volume are absorbed by the interparticle pore space is a function of the structural features of the particle and pore fabric, the total void volume of the specimen, the ratio of interparticle volume to interlayer volume, and the corresponding bulk compressibility of the specimen.

https://doi.org/10.1346/CCMN.2006.0540412 Published online by Cambridge University Press

Microstructural analysis of multi-step results

The microstructural model developed above was used to model the evolution of interlayer and interparticle pore volume for Na^+ and Ca^{2+} specimens from the multi-step testing series. Figure 8a shows interlayer, interparticle, and total void ratio computed during hydration and subsequent dehydration for the Na^+ specimen. The total void ratio was computed from axial deformation and water content at steady state for each RH increment under the assumption of isotropic volume change. Interlayer void ratio was computed using equation 8 from estimates of interlayer separation 2δ as a function of RH determined by interpolating basal spacing measurements reported by Chipera *et al.* (1997) for Na^+-exchanged SAz-1 smectite (Table 1). Interparticle void ratio was computed as the difference between the total and interlayer void ratios at each increment.

The initial interlayer volume is zero, which corresponds to the fully dehydrated condition sustained for RH values <~10%. Relative humidity of ~10–30% marks the transition to the one-layer hydrate state. Corresponding changes in specimen volume (Figure 4), however, are relatively small, indicating that the increase in basal spacing associated with the zero-to-one layer transition is partially absorbed by the larger-scale voids. This loss of interparticle void volume is reflected by the significant reduction in interparticle void ratio that occurs. At RH = 27.5%, interlayer volume has increased from 0 to 34% of the total void volume and interparticle volume has decreased from 100 to 66% of the total void volume. The ratio of interlayer volume to interparticle volume has increased from 0 to 51%. Interlayer spacing from ~30% RH to 60% RH is relatively stable, yet bulk volume change occurs (Figure 4) as water continues to be adsorbed (Figure 3a). This volume change may be associated with continued filling of the first H_2O layer, interstratification of multiple hydration states within the specimen, partial disassociation of the 7-to-8-layer substacks within the quasicrystals, or adsorption in the interparticle void space. The last mechanism suggests that the interparticle pore volume may expand to accommodate the additional water, which is reflected by the gradual and fairly constant increase in interparticle void ratio. RH from ~60 to 80% marks transition to the two-layer hydrate state. Here, a slight increase in interparticle void volume occurs and a significant amount

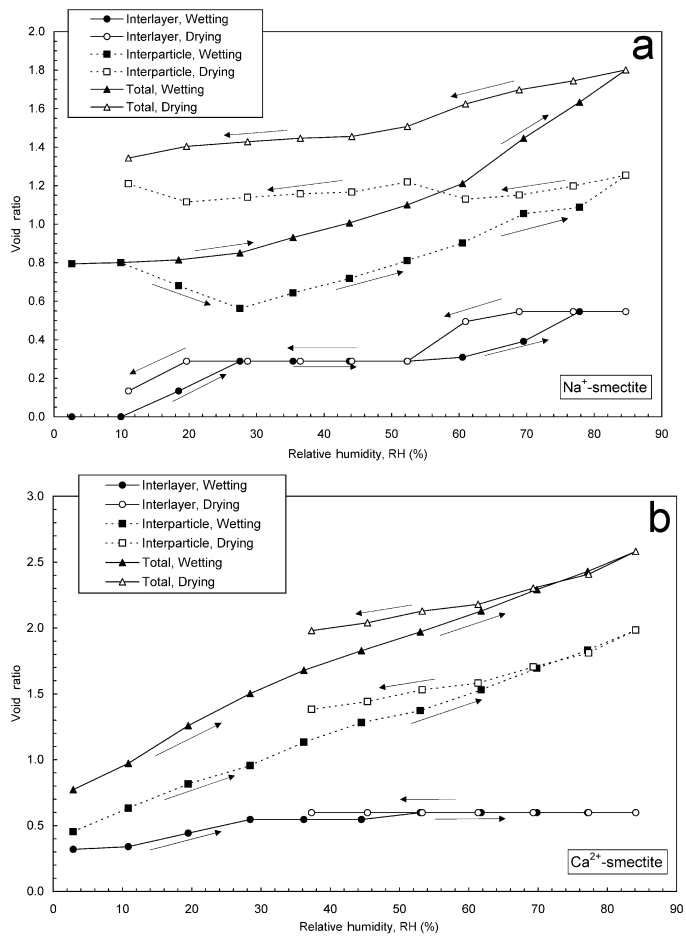

Figure 8. Evolution of interlayer, interparticle, and total void ratio for multi-step specimens: (a) Na^+-smectite and (b) Ca^{2+}-smectite.

https://doi.org/10.1346/CCMN.2006.0540412 Published online by Cambridge University Press

Table 1. Basal spacing and interlayer separation as function of RH for microstructural modeling of multi-step sorption results.

	Na^+			Ca^+	
RH (%)	d_{001} (Å)*	2δ (Å)	RH (%)	d_{001} (Å)*	2δ (Å)
Wetting					
2.6	9.7	0.0	2.9	12.8	3.1
9.9	9.7	0.0	10.8	13.0	3.3
18.5	11.0	1.3	19.5	14.0	4.3
27.5	12.5	2.8	28.4	15.0	5.3
35.4	12.5	2.8	36.2	15.0	5.3
43.8	12.5	2.8	44.5	15.0	5.3
52.3	12.5	2.8	53.0	15.5	5.8
60.5	12.7	3.0	61.8	15.5	5.8
69.5	13.5	3.8	69.8	15.5	5.8
77.8	15.0	5.3	77.2	15.5	5.8
84.7	15.0	5.3	84.1	15.5	5.8
Drying					
76.9	15.0	5.3	77.3	15.5	5.8
68.9	15.0	5.3	69.3	15.5	5.8
60.9	14.5	4.8	61.3	15.5	5.8
52.3	12.5	2.8	53.3	15.5	5.8
44.1	12.5	2.8	45.4	15.5	5.8
36.5	12.5	2.8	37.3	15.5	5.8
28.7	12.5	2.8			
19.6	12.5	2.8			
11.0	11.0	1.3			

* Basal spacing interpolated from the humidity-controlled XRD results of Chipera *et al.* (1997)

of bulk volume change occurs, which is shown in Figure 5a by the large peak in Δh/ΔRH at ~70% RH. Following the conceptual framework, the one-to-two layer transition is more effectively translated to bulk volume change because the interparticle void volume prior to the transition represents a lesser percentage of the total void volume (74% of the total void volume at RH = 60.5% compared with 100% at RH = 9.9%). In addition, if sorption has occurred in the interparticle voids from 30% to 60% RH, then the interparticle voids are partially filled with water and their compressibility may be significantly reduced.

During drying, the interlayer volume transitions back to near zero as the interlayer dehydrates. Interparticle void ratio increases slightly with the two-to-one (~60% RH) and one-to-zero (~20% RH) transitions, indicating an increasing contribution of interparticle voids to the total void volume. The interparticle void ratio maintains a relatively high value through the end of the drying cycle due to hysteresis in the total volume change response. The final interparticle void ratio is 53% greater than its initial value. This significant change implies that the unrecovered total volume upon drying resides primarily in newly expanded interparticle pores.

For initially dry clays, the interparticle voids are most significantly altered upon first expansion because the initial interlayer pore volume is at a minimum. For highly compacted clays, the interparticle voids are most significantly altered upon first expansion because the initial interparticle void volume is also at a minimum. Numerous macroscopic studies, for example, have shown that compacted expansive clay exhibits irrecoverable macroscopic volume changes upon initial wetting-drying cycles but volume changes are reversible after subsequent cycles, an observation typically attributed to alterations in particle or pore fabric (*e.g.* Gens and Alonso, 1992; Tripathy *et al.*, 2002). Results from the current model provide insight by clarifying that, within the crystalline swelling regime, these fabric alterations may occur primarily in the larger-scale interparticle void space. If, on the other hand, the interlayers fully disassociate at higher water contents within the osmotic swelling regime, then unrecovered total volume changes may be more significantly governed by irreversible changes in the interlayer fabric. Laird *et al.* (1995) reviewed several explanations for the causes of hysteresis in interlayer swelling and examined hysteresis in smectites using XRD to measure basal spacing. Sources were attributed to mechanisms termed intrinsic and extrinsic, where the former is associated with work needed to overcome rigidity of the clay-water system for each pair of expanding layers and the latter is associated with work required to overcome additional rigidity imposed by surrounding layers comprising larger fabric units (quasicrystals). If we consider macroscopic volume change hysteresis in a similar context, the work associated with altering the interparticle pore volume during swelling is analogous to the extrinsic mechanism noted above, and therefore is expected to be greater for hydrating systems where alterations in interparticle void volume more readily occur.

Figure 8b shows the evolution of interlayer, interparticle, and total void ratio for the multi-step Ca^{2+} specimen. Component and total void ratios were computed in the same manner as for the Na^+ specimen, with the exception that the Ca^{2+} specimen was assumed to initially reside at the one-layer hydration state, and therefore has a non-zero initial interlayer volume. The initial interlayer volume is 41% of the total void volume and the ratio of interlayer to interparticle volume is 70%. Subsequent interlayer volumes were computed from interlayer separations summarized on Table 1, where transition from the one-layer state to the two-layer state initiates immediately and is complete by RH of ~30%. Interlayer spacing for the remainder of the hydration cycle is relatively constant. As noted in Figure 4, the one-to-two layer transition is marked by significant bulk volume change, which results in an increase in interlayer void ratio from 0.32 to 0.55. Interparticle void volume increases significantly during the transition, thus indicating a necessary expansion of the interparticle voids to accommodate the interlayer volume change (V_{IP} increases from 26% to 38% of V_t). By comparison, the

https://doi.org/10.1346/CCMN.2006.0540412 Published online by Cambridge University Press

interparticle void volume of the Na^+ specimen during the same (one-to-two layer) transition increases from 41 to 45% of the total volume. The larger increase for the Ca^{2+} specimen is attributed to the fact that the volume of the interparticle voids prior to the transition is relatively small. The continuing increase in interparticle void volume within the relatively stable two-layer regime implies continuing adsorption in the interparticle void space, which must expand to accommodate the additional water.

Microstructural analysis of single-step results

Results from the single-step testing series may be considered to examine the role of initial particle fabric on changes in interlayer and interparticle void volume during hydration. For example, Figure 9 shows the percentage change in interparticle void ratio (Δe_{IP}) as a function of initial interparticle void ratio (e_{IPi}) for compacted specimens equilibrated to 93% RH. Initial interparticle void ratio was calculated from the total void ratio measured after compaction and interlayer void ratios corresponding to the zero-layer and one-layer separation distances for the Na^+ and Ca^{2+} specimens, respectively. Interparticle void ratio at RH = 93% was calculated for both clays from the total void ratio measured after equilibrium and interlayer void ratio corresponding to the two-layer hydration state.

Figure 9 indicates a clear relationship between initial interparticle void volume and its subsequent change upon hydration. The change is greatest for specimens initially compacted to relatively dense conditions, which is consistent with the conceptual framework where the larger-scale voids must expand significantly to accommodate interlayer volume changes if the initial volume of larger-scale voids is relatively small. It is also notable that the relationship appears to be essentially independent of cation type, suggesting that alterations to the larger-scale pore fabric upon hydration depend primarily on the initial volume fraction of the interparticle pores rather than the thickness and distribution of the quasicrystals as influenced by cation type. The static compaction results (Figure 2) indicate that the bulk compressibility of the Na^+ and Ca^{2+} specimens is similar (and nearly identical for total void ratio < ~0.84). The compaction curves primarily reflect compression of the interparticle voids. Thus, the interparticle compressibility of the specimens may be considered similar, which supports the argument that alterations to the larger-scale pore fabric govern bulk volume change and suggests that these alterations are comparable for specimens initially at the same interparticle void volume and subject to the same degree of interlayer swelling. Finally, an initial interparticle void ratio near 1.0 appears to represent ideal conditions for minimizing subsequent alterations to interparticle void volume. This observation may have practical implications, as many aspects of macroscopic behavior (*e.g.* permeability, compressibility) are governed primarily by the larger-scale voids. Changes in macroscopic behavior, therefore, are largely influenced by changes in the volume and fabric of these voids and in many practical applications are undesirable. Additional experiments are required to support these trends for a wide range of specimen types, compaction conditions, and confining conditions.

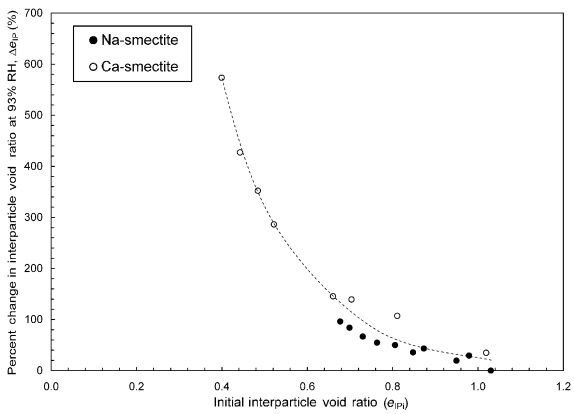

Figure 9. Relationship between initial interparticle void ratio and change in interparticle void ratio at RH = 93%.

SUMMARY AND CONCLUSIONS

Multi-step and single-step water-vapor sorption experiments were conducted to quantify the bulk volume change of compacted expansive clay specimens within the crystalline swelling regime. The effects of interlayer cation type and initial compaction conditions were examined by comparing results for natural Na^+-smectite and Ca^{2+}-smectite specimens statically compacted over a range of initial particle packing densities. Transitions in interlayer hydration states are reflected in the general shape and slope of the sorption isotherms and the corresponding relationships between RH and macroscopic volume change. Analysis of the slope of volume change responses provides a basis to interpret large increases in volume change occurring within specific RH regimes as the macroscopic manifestation of crystalline swelling. Additional testing with a smaller RH increment (<10%) may more clearly elucidate the apparent transition regimes. The requirement for relatively long testing durations (70−150 h/step), however, represents a limitation of the multi-step testing system and a balance between specimen mass (which governs test duration), corresponding specimen volume, and the necessary precision in volume change measurements must be maintained.

Maximum axial strains of 16.3% and 26.4% were obtained under free swelling (unconfined) conditions at the highest increment in RH (~ 85%) for the Na^+ and Ca^{2+} specimens, respectively, corresponding to volumetric strains of 57.9% and 102.0%. Unrecovered volume changes were sustained during drying. Volume

https://doi.org/10.1346/CCMN.2006.0540412 Published online by Cambridge University Press

changes for Ca^{2+}-smectite specimens equilibrated to 93% RH in single-step sorption experiments were significantly greater than for the Na^{+}-smectite over the entire range of compaction conditions considered. Loosely compacted specimens result in lesser amounts of bulk volume change for both clay types.

Results were interpreted in light of a conceptual framework based on previous SEM and TEM observations of particle and pore fabrics for Na^{+}- and Ca^{2+}-smectite (Tessier, 1990). For the Na^{+} system, where the interparticle voids initially represent a significant portion of the total void volume, interlayer volume changes are more effectively absorbed by the interparticle void space and the translation of crystalline swelling to macroscopic volume change is inefficient. For the Ca^{2+} fabric system, where the interparticle voids initially represent a smaller portion of the total void volume, interlayer volume changes are less effectively absorbed by the interparticle void space and the translation of crystalline swelling to macroscopic volume change is more efficient.

A pore-scale microstructural model was developed to extend the conceptual framework and quantitatively assess the evolution in interlayer and interparticle void volume during hydration and dehydration cycles within the crystalline swelling regime. The model is general and may be extended to examine fabric evolution at larger separations associated with the osmotic swelling regime if these separations are measured or estimated using existing theory. Results from the multi-step testing series were modeled to indicate that the relatively small bulk volume changes observed for the Na^{+} specimen may be more specifically attributed to a loss of interparticle void volume as expanding quasicrystals encroach into their surrounding void space during the zero-to-one layer transition. Unrecovered volume changes during drying are attributed to alterations in the interparticle voids required to accommodate the swelling process, providing insight for understanding more general volume change hysteresis phenomena noted for expansive clays in the literature. Quantitative analysis of the single-step results provides additional support to the conceptual framework by indicating that specimens initially compacted to relatively dense conditions exhibit greater alterations to interparticle pore space during hydration. Relationships between initial interparticle void volume and the percent change in interparticle void volume upon hydration appear to be independent of cation type, suggesting that alterations to the larger-scale pore fabric depend primarily on the initial volume fraction of the interparticle pores rather than the thickness and distribution of the quasicrystals. Initial interparticle void ratio near 1.0 appears to represent ideal conditions for minimizing subsequent changes in interparticle void volume during hydration during crystalline swelling. The results reported here provide new insight into how initial clay fabric and subsequent changes in interlayer and interparticle pore volume influence bulk volume change and hysteresis in the crystalline swelling regime.

REFERENCES

ASTM (2000) *Annual Book of ASTM Standards*, Vols 4.08 and 4.09, D-18 Committee on Soils and Rock. American Society for Testing and Materials, West Conshohocken, Pennsylvania.

Aylmore, L.A.G. and Quirk, J.P. (1971) Domains and quasicrystalline regions in clay systems. *Soil Science Society of America Proceedings*, **35**, 652–654.

Barshad, I. (1949) The nature of lattice expansion and its relation to hydration in montmorillonite and vermiculite. *American Mineralogist*, **34**, 675–684.

Berend, I., Cases, J., Francois, M., Uriot, J., Michot, L., Maison, A. and Thomas, F. (1995) Mechanism of adsorption and desorption of water vapor by homoionic montmorillonites. *Clays and Clay Minerals*, **43**, 324–336.

Bishop, J.L., Pieters, C.M. and Edwards, J.O. (1994) Infrared spectroscopic analyses on the nature of water in montmorillonite. *Clays and Clay Minerals*, **42**, 702–716.

Boek, E.S., Coveney, P.V. and Skipper, N.T. (1995) Molecular modeling of clay hydration. A study of hysteresis loops in the swelling curves of Na-montmorillonite. *Langmuir*, **11**, 4629–4631.

Cases, J.M., Berend, I., Besson, G., Francois, M., Uriot, J.P., Thomas, F. and Poirier, J.E. (1992) Mechanism of adsorption and desorption of water vapor by homoionic montmorillonite. I. The sodium exchanged form. *Langmuir*, **8**, 2730–2739.

Cebula, D.J., Thomas, R.K., Middleton, S., Ottewill, R.H. and White, J.W. (1979) Neutron diffraction from clay/water systems. *Clays and Clay Minerals*, **27**, 39–52.

Chang, F.R.C., Skipper, N.T. and Sposito, G. (1995) Computer simulation of interlayer molecular structure in sodium montmorillonite hydrates. *Langmuir*, **11**, 2734–2741.

Chipera, S.J., Carey, J.W. and Bish, D.L. (1997) Controlled-humidity XRD analyses: Application to the study of smectite expansion/contraction. Pp. 713–721 in: *Advances in X-ray Analysis*, **36** (J.V. Gilfrich *et al*., editors). Plenum Press, New York.

Collis-George, N. (1955) The hydration and dehydration of Na-montmorillonite (Belle Fourche). *Journal of Soil Science*, **6(1)**.

Delage, P., Howat, M.D. and Cui, Y.J. (1998) The relationship between suction and swelling properties in a heavily compacted unsaturated clay. *Engineering Geology*, **50**, 31–48.

Delville, A. and Letellier, M. (1995) Structure and dynamics of simple liquids in heterogeneous conditions: an NMR study of the clay water interface. *Langmuir*, **11**, 1361–1367.

Del Pennino, U., Mazzega, E. and Valeri, S. (1981) Interlayer water and swelling properties of monoionic montmorillonites. *Journal of Colloid and Interface Science*, **84**, 301–309.

Eberl, D.D., Drits, V.A. and rodoñ, J. (1996) *MUDMASTER; a program for calculating crystallite size distributions and strain from the shapes of X-ray diffraction peaks.* US Geological Survey Open File Report 96-0171.

Farmer, V.C. and Russell, J.D. (1971) Interlayer complexes in layer silicates. The structure of water in lamellar ionic solutions. *Transactions of the Faraday Society*, **67**, 2737–2749.

Gens, A. and Alonso, E.E. (1992) A framework for the behavior of unsaturated expansive clays. *Canadian Geotechnical Journal*, **29**, 1013–1032.

https://doi.org/10.1346/CCMN.2006.0540412 Published online by Cambridge University Press

Gillery, F.H. (1959) Adsorption-desorption characteristics of synthetic montmorillonoids in humid atmospheres. *American Mineralogist*, **44**, 806–818.

Grandjean, J. and Laszlo, P. (1989) Deuterium nuclear magnetic resonance studies of water molecules restrained by their proximity to a clay surface. *Clays and Clay Minerals*, **37**, 403–408.

Huang, W., Bassett, W.A. and Wu, T. (1994) Dehydration and hydration of montmorillonite at elevated temperatures and pressures monitored using synchrotron radiation. *American Mineralogist*, **79**, 683–691.

Hawkins, R.K. and Egelstaff, P.A. (1980) Interfacial water structure in montmorillonite from neutron diffraction experiments. *Clays and Clay Minerals*, **28**, 19–28.

Karaborni, S., Smit, B., Heidug, W. and van Oort, E. (1996) The swelling of clays: molecular simulations of the hydration of montmorillonite. *Science*, **271**, 1102–1104.

Keren, R. and Shainberg, I. (1975) Water vapor isotherms and heat of immersion of Na/Ca-montmorillonite systems – I: Homoionic clay. *Clays and Clay Minerals*, **23**, 193–200.

Kittrick, J.A. (1969) Interlayer forces in montmorillonite and vermiculite. *Soil Science Society of America Proceedings*, **33**, 217–222.

Laird, D.A. (1996) Model for crystalline swelling of 2:1 phyllosilicates. *Clays and Clay Minerals*, **44**, 553–559.

Laird, D.A., Shang, C. and Thompson, M.L. (1995) Hysteresis in crystalline swelling of smectites. *Journal of Colloid and Interface Science*, **171**, 240–245.

Likos, W.J. (2004) Measurement of crystalline swelling in expansive clay. *Geotechnical Testing Journal*, **27**, 540–546

MacEwan, D.M.C. and Wilson, M.J. (1980) Interlayer and intercalation complexes of clay minerals. Pp. 197–248 in: *Crystal Structures of Clay Minerals and their X-ray Identification* (G.W. Brindley and G. Brown, editors). Monograph **5**, Mineralogical Society, London.

Mooney, R.W., Keenan, A.G. and Wood, L.A. (1952) Adsorption of water vapor by montmorillonite. II. Effect of exchangeable ions and lattice swelling as measured by X-ray diffraction. *Journal of American Chemical Society*, **74**, 1371–1374.

Moore, D.M., and Reynolds, R.C. (1997) *X-ray Diffraction and the Identification and Analysis of Clay Minerals*, Oxford University Press, New York.

Mystkowski, K., Środoń, J. and Elsass, F. (2000) Mean thickness and thickness distribution of smectite crystallites. *Clay Minerals*, **35**, 545–557.

Norrish, K. (1954) The swelling of montmorillonite. *Transactions of the Faraday Society*, **18**, 120–134.

Poinsignon, C., Estrade-Schwarzckopf, J., Conard, J. and Dianoux, A.J. (1987) Water dynamics in the clay water system: A quasi-elastic neutron scattering study. Pp. 284–291 in: *Proceedings of the International Clay Conference* (L.G. Schultz, H. Van Olphen and F.A. Mumpton, editors). The Clay Minerals Society, Denver, Colorado.

Posner, A.M. and Quirk, J.P. (1964) Changes in basal spacing of montmorillonite in electrolyte solutions. *Journal of Colloid Science*, **19**, 798–812.

Powell, D.H., Tongkhao, K., Kennedy, S.J. and Slade, P.G. (1997) A neutron diffraction study of interlayer water in sodium Wyoming montmorillonite using a novel difference method. *Clays and Clay Minerals*, **45**, 290–294.

Rouquerol, F. (1999) *Adsorption by Powders and Porous Solids: Principles, Methodology, and Applications*. Academic Press, San Diego, California.

Slade, P.G. and Quirk, J.P. (1991) The limited crystalline swelling of smectites in $CaCl_2$, $MgCl_2$, and $LaCl_3$. *Journal of Colloid and Interface Science*, **144**, 18–26.

Slade, P.G., Quirk, J.P. and Norrish, K. (1991) Crystalline swelling of smectite samples in concentrated NaCl solutions in relation to layer charge. *Clays and Clay Minerals*, **39**, 234–238.

Sposito, G. and Prost, R. (1982) Structure of water adsorbed on smectites. *Chemical Reviews*, **82**, 553–573.

Sposito, G., Park, S.-H., and Sutton, R. (1999) Monte Carlo simulation of the total radial distribution function for interlayer water in sodium and potassium montmorillonites. *Clays and Clay Minerals*, **47**, 192–200.

Tessier, D. (1990) Behavior and microstructure of clay minerals. Pp. 387–415 in: *Soil Colloids and their Associations in Aggregates* (M.F. DeBoodt, M.H.B. Hayes and A. Herbillon, editors). Plenum Press, New York.

Tripathy, S., Subba Rao, K.S. and Fredlund, D.G. (2002) Water content – void ratio swell-shrink paths of compacted expansive soils. *Canadian Geotechnical Journal*, **39**, 938–959.

Weiss Jr, C.A. and Gerasimowicz, W.V. (1996) Interaction of water with clay minerals as studied by 2H Nuclear Magnetic Resonance spectroscopy. *Geochimica et Cosmochimica Acta*, **60**, 265–271.

(*Received 26 August 2005; revised 7 February 2006; Ms. 1087; A.E. Will P. Gates*)